Journal of Cardiovascular Translational Research

Right ventricular function after pulmonary artery banding: adaptive processes assessed by CMR and conductance catheter measurements in sheep

--Manuscript Draft--

Manuscript Number:	CATR-D-18-00200R2
Full Title:	Right ventricular function after pulmonary artery banding: adaptive processes assessed by CMR and conductance catheter measurements in sheep
Article Type:	Original Article
Keywords:	Cardiac Magnetic Resonance; hemodynamics; Pulmonary artery hypertension; Pulmonary artery banding; Conductance catheter
Corresponding Author:	Hubert Gufler Martin-Luther-Universitat Halle-Wittenberg Halle (Saale), GERMANY
Corresponding Author Secondary Information:	
Corresponding Author's Institution:	Martin-Luther-Universitat Halle-Wittenberg
Corresponding Author's Secondary Institution:	
First Author:	Hubert Gufler
First Author Secondary Information:	
Order of Authors:	Hubert Gufler
	Sabine Niefeldt, M.D.
	Johannes Boltze, PhD
	Stephanie Prietz, M.D.
	Christian Klopsch, M.D.
	Sabine Wagner, M.D.
	Brigitte Vollmar, Prof.
	Can Yerebakan, M.D.
Order of Authors Secondary Information:	
Funding Information:	
Abstract:	This experimental study describes the adaptive processes of the right ventricular (RV) myocardium after pulmonary artery banding (PAB) in sheep evaluated by cine cardiac magnetic resonance (CMR), phase-contrast CMR (PC-CMR) and conductance catheter. Seven sheep were subjected to CMR three months after PAB. Conductance catheter was performed before and three months after PAB. Four non-operated healthy age-matched animals served as controls. Higher RV masses ($p < 0.01$), elevated RV end-systolic volumes ($p < 0.01$), and lower RV ejection fraction ($p < 0.01$) were observed in the operated group. The time-to-peak pulmonary artery flow was longer in the banding group ($p < 0.01$). RV-maximal pressure and RV-end diastolic pressure correlated with the time-to peak flow in the pulmonary artery ($r = -77$ and -0.71, respectively). In summary, PAB caused RV hypertrophy, increased myocardial contractility, decreased RV-EF and cardiac output. The time-to-peak pulmonary artery flow correlated with RV pressures.

Right ventricular function after pulmonary artery banding: adaptive processes assessed by CMR and conductance catheter measurements in sheep

[1]Hubert Gufler, M.D; [2]Sabine Niefeldt, M.D.; [3]Johannes Boltze, Prof.; [2]Stephanie Prietz, M.D; [2]Christian Klopsch, M.D.; [1]Sabine Wagner, M.D.; [4]Brigitte Vollmar, Prof.; [2]Can Yerebakan, M.D.

[1]Department of Diagnostic and Interventional Radiology, University Clinic, 10857 Rostock, Schillingallee 35, Germany
[2]Department of Cardiac Surgery, University Clinic, 10857 Rostock, Schillingallee 35, Germany
[3]Fraunhofer Research Institution for Marine Biotechnology, Department of Medical Cell Technology and Institute for Medical and Marine Biotechnology, University of Lübeck, Lübeck, Germany
[4]Institute for Experimental Surgery, Rostock University Medical Center, 18057 Rostock, Schillingallee 69a, Germany

Short title: RV function after pulmonary artery banding

Word count: 4003

Correspondence to:
Dr. Hubert Gufler
Present/permanent address:
Clinic and Policlinic of Radiology,
Martin-Luther University Halle-Wittenberg,
Ernst-Grube-Str. 40, 06120 Halle Germany
Phone: 0049 0345 557 2441
Fax: 0049 0345 557 2157
E-mail: hgufler@gmx.de

Abstract

This experimental study describes the adaptive processes of the right ventricular (RV) myocardium after pulmonary artery banding (PAB) evaluated by cine cardiac magnetic resonance (CMR), phase-contrast CMR (PC-CMR), and conductance catheter. Seven sheep were subjected to CMR three months after PAB. Conductance catheter measurements were performed before and three months after PAB. Four nonoperated, healthy, age-matched animals served as controls. Higher RV masses ($p < 0.01$), elevated RV end-systolic volumes ($p < 0.05$), and lower RV ejection fraction ($p < 0.01$) were observed in the operated group. The time-to-peak pulmonary artery flow was longer in the banding group ($p < 0.01$). RV maximal pressure and RV end-diastolic pressure correlated with the time-to-peak flow in the pulmonary artery ($r = -0.70$ and -0.69, respectively).

In summary, PAB caused RV hypertrophy, increased myocardial contractility, and decreased RV-EF and cardiac output. The time-to-peak pulmonary artery flow correlated with RV pressures.

Key words: Cardiac magnetic resonance; Hemodynamics; Pulmonary artery hypertension; Pulmonary artery banding; Conductance catheter

Abbreviations:

RV = right ventricle

PA = pulmonary artery

PAB = pulmonary artery banding

CMR = cardiac magnetic resonance

PC-CMR = phase contrast cardiac magnetic resonance

EF = ejection fraction

ESV = end-systolic volume

EDV = end-diastolic volume

SV = stroke volume

RV-P_{max} = RV maximal systolic pressure

RV-EDP = right ventricular end-diastolic pressure

RV-ESP = right ventricular end-systolic pressure

RV-dP/dt_{max} = right ventricular maximum rate of pressure rise

RV-dP/dt_{min} = right ventricular minimum rate of pressure rise

RV-CO = right ventricular cardiac output

RV-EDPVR = RV end-diastolic pressure volume relationship

RV-ESPVR = RV end-systolic pressure volume relationship

RV-PRSW = RV preload recruitable stroke work

SSFP = steady-state free precession

ECG = electrocardiogram

TVA = tricuspid valve annulus

TVA-MD = tricuspid valve annulus maximal longitudinal displacement

TVA-V_{max} = tricuspid valve annulus maximal velocity

TVA-VED = tricuspid valve annulus maximal velocity at end diastole

TTP = time-to-peak

Introduction

Primary repair is the curative aim in infants with complex congenital heart diseases. However, first-stage palliative treatment with pulmonary artery banding (PAB) followed by complete repair at a later time point may represent an alternative surgical option for some patients who are not suitable for primary repair [1, 2]. For example, in selected patients in whom the great arteries are transposed, a period of preconditioning by PAB is required prior to anatomic correction [3]. The timely detection of right ventricular (RV) dysfunction is crucial for overall prognosis of these patients. The mechanisms underlying the progression from compensated RV hypertrophy to RV failure are not fully understood. Several adaptive processes are induced by PAB: humoral responses, myocyte hypertrophy, myocyte hyperplasia, changes in the extracellular matrix, and shift to lengthened sarcomeres [4,5]. Fibrosis and an insufficient increase in capillary density are thought to be responsible for ventricular dysfunction and eventually ventricular failure [6,7].

RV pressure-volume analysis remains the gold standard to assess the contractility state of the RV and its response to pressure overload, but it is invasive and mostly used in experimental studies [8-10]. The key parameters obtained by conductance catheter are end-diastolic pressure relationship (EDPVR) and end-systolic pressure relationship (ESPVR), the former being a sensitive parameter of early diastolic ventricular dysfunction and the latter the optimal quantifying parameter of contractility [11, 12]. Noninvasive methods to determine the contractility state of the LV, such as strain, strain rate, and wall stress, have been developed for both echocardiography and cardiac magnetic resonance (CMR) [13-16]. However, it is a challenge to measure these parameters in the RV because of its complex anatomy and contraction pattern.

The objectives of the present experimental study were to assess the RV responses to chronic pressure overload induced by PAB using CMR and conductance catheter and to find CMR parameters that are suitable to detect RV failure noninvasively at an early stage after PAB.

Materials and Methods

Animal model

PAB via left anterior thoracotomy was performed in 7 four-month old female domestic sheep. Prior to the surgical procedures, the animals received an intramuscular injection of 0.5 mg/kg xylazine (Rompun 2%, Bayer Vital GmbH, Leverkusen, Germany) and 10 mg/kg ketamine 10% (Ketamin 10%, Bela-Pharm GmbH & Co. KG, Vechta, Germany), followed by intubation. Inhalation anesthesia was maintained by 1.5 - 2.5% isoflurane delivered through a ventilator (Excel 210 SE, Ohmeda-BOC Group, Madison, WI, USA). The degree of main pulmonary artery (PA) tightening was controlled by directly measuring RV pressures using a conductance catheter (Millar Instruments, Houston, TX, USA). The target of RV maximal systolic pressure (RV-Pmax) was set to 50 - 60% above baseline level [17].

Conductance catheter measurements

Conductance catheter measurements were performed via left anterior thoracotomy before PAB and via median sternotomy 3 months after PAB. The following parameters were determined by analyzing pressure-volume loops: maximal RV pressure (RV-Pmax), end-diastolic and end-systolic pressure (RV-Ped, RV-Pes), maximum and minimum rates of pressure rise (RV-dP/dtmax, RV-dP/dtmin), and cardiac output of the RV (RV-CO). Furthermore, the slopes of end-diastolic pressure-volume relation (RV-EDPVR), end-systolic pressure-volume relation (RV-ESPVR), and the preload-recruitable stroke work (RV-PRSW) were calculated after occluding the inferior vena cava by using a 23-mm balloon catheter

(Fogarty Occlusion Catheter, Edward Lifesciences LLC, Irvine, CA, USA). End-systolic elastance (Ees) was derived from pressure-volume loops. Arterial elastance (Ea) was calculated as end-systolic pressure divided by stroke volume. The right ventricular – arterial coupling was defined as the ratio of Ees to Ea.

Cardiac magnetic resonance

CMR was performed in seven female sheep 3 months after PAB and in four female healthy control animals, age-matched with the animals 3 months after PAB. CMR was carried out under anesthesia and mechanical ventilation on a 1.5-Tesla scanner (Magnetom Avanto, Siemens Healthineers, Erlangen, Germany) using a phased-array cardiac coil and a vector electrocardiographic system for cardiac gating. All measurements were taken at end-expiration with the ventilator turned off to minimize motion artifacts. Steady-state free precession (SSFP) cine images were obtained in the standard views for both ventricles, including 10 – 12 contiguous, short-axis, 6-mm-thick slices encompassing both ventricles from base to apex.

Phase-contrast CMR (PC-CMR) was employed to measure the flow in 5-mm-thick slices orthogonally to the course of the PA and the aorta. Twenty-eight frames were acquired per average cardiac cycle. Velocity-encoding gradients were set to cover a dynamic range from -200 to 200 cm/s, with a sequential increase in maximum range if aliasing artifacts were encountered. The maximal blood flow, the maximal flow velocity, and the changes in vessel diameter throughout the cardiac cycle were measured at the banding area and 1 cm above the aortic valve.

Cardiac magnetic resonance data analysis

Short-axis slices of both ventricles were loaded into a volume evaluation tool (Argus software, Leonardo, Siemens Healthcare, Erlangen, Germany). Endocardial contours of both

ventricles were manually outlined on the end-diastolic and end-systolic frames and epicardial contours on the end-diastolic frames. End-systolic volumes (ESV), end-diastolic volumes (EDV), and stroke volumes (SV) along with the ventricular muscle masses were calculated for each ventricle separately.

The tricuspid valve annulus (TVA) displacement and velocity were determined to assess the RV diastolic function – analogous to the method describing the mitral valve annulus movement to assess the LV diastolic function [18-20]. TVA maximal longitudinal displacement (TVA-MD), TVA maximal velocity in diastasis (TVA-VDS) – reflecting the quiescent phase of diastole - and TVA maximal velocity in early diastole (TVA-VED) were measured on 4-chamber cine images using a MATLAB platform (The MathWorks, Natick, Massachusetts, USA). The longitudinal displacement and the displacement velocity of the TVA were measured relative to a reference line drawn from the RV apex to the midpoint of the TVA for each of the 20 phases throughout the cardiac cycle.

Finally, the PC-CMR data sets were loaded into the Argus flow evaluation tool. The inner contours of the main PA at the banding site and of the aorta were outlined in each cardiac phase on the magnitude images. Peak flow, peak velocity, time-to-peak flow, and cross-sectional areas were calculated automatically. The time-to-peak flow was defined as the time interval from the beginning of the anterograde flow upslope in systole to the peak systolic flow.

Statistical Analysis

Statistical analysis was performed using SPSS software (Statistical Package for the Social Sciences, Chicago, Illinois). CMR parameters were reported as mean ± standard deviation (SD). Since the group sizes were too small to reliably run tests on Gaussian distribution, all pairwise comparisons were performed by applying the nonparametric Mann-Whitney U test. Statistical significance was assumed for $p < 0.05$. Pearson's correlation coefficients were

calculated to assess the relationship between continuous variables. For interobserver variability assessment, data sets were processed independently by two raters, blinded to each other's measurements. For intraobserver variability, 12 months after the initial analysis, one of the evaluators blindly and randomly reprocessed the data sets. Agreement was expressed by the Pearson's correlation coefficient and Bland-Altman analysis.

Results

Body weight and age of animals

The body weight of the animals in the operated group was 39 ± 1.34 kg; the body weight of those in the healthy control group was 42.25 ± 1.89 kg ($p = 0.078$). The age of the animals in the operated group was 25.28 ± 0.75 weeks; the age of the animals in the healthy control group was 24.50 ± 0.57 weeks ($p = 0.089$).

Conductance catheter measurements

The results of the conductance catheter measurements are summarized in Table 1. RV cardiac output decreased significantly by 36% after PAB, which was due to a decrease in RV-SV as heart rate did not change significantly. On the other hand, a significant increase in myocardial contractility was observed since both the slope of the RV-ESPVR and the RV-PRSW increased after the banding. The slope of RV-EDPVR decreased significantly after PAB, indicating that diastolic compliance was raised. No statistically significant differences were found for RV-Ped, RV-Pes, RV-Pmax, dP/dtmax, and dP/dtmin before and 3 months after PAB. While Ea remained nearly unchanged after PAB, Ees increased significantly after PAB; as a result, the ratio Ees/Ea increased.

Cardiac magnetic resonance measurements

The results of MR-based RV and left ventricle (LV) volume measurements are summarized in Table 2. The average muscle mass of the RV was significantly higher in the PAB group. The RV ejection fraction (RV-EF) was significantly lower in the PAB group than in the healthy

controls, which could mainly be attributed to an increased RV-ESV. The RV-EDV were not significantly different when comparing the means in the PAB group and the healthy controls.

No statistically significant difference was found between PAB and the healthy control animals for TVA-MD (11.9 ± 3.8 mm versus 11.8 ± 2.2 mm; p = 0.91) and TVA-VED (4.1 ± 0.1 cm/s versus 4.6 ± 1.8 cm/s; p = 0.27), with TVA-VDS (0.7 ± 1.1 cm/s versus 0.1 ± 1.3 cm/s; p = 0.053), values tending to be higher in the PAB group.

The time difference between the peak flow in the PAB area and the peak flow in the aorta was significantly different from healthy control subjects, indicating a shift to the right of the PA peak flow in the PAB group. In detail, the time-to-peak flow in the PA was 195.4 ± 77.6 ms compared to 88.8 ± 14.2 ms in the healthy control group (p < 0.01) (Figure 1). RV Pmax and Ped correlated negatively with the time-to-peak flow in the pulmonary artery (r = -0.70 and -0.69, respectively (Figure 2). The maximal flow velocity at the PAB area was 2.4 times higher than in the healthy control group (172 ± 37.8 cm/s and 70.8 ± 27.0 cm/s, respectively, p < 0.01).

Intraobserver variability was $r = 0.98$, and bias -0.39 ± 5.3 ml for RV-EDV; $r = 0.97$, and bias -0.55 ± 3.7 ml for RV-ESV; and $r = 0.94$, and bias -0.45 ± 6.5 g for RV-mass. Interobserver variability was $r = 0.98$, and bias -0.93 ± 4.4 ml for RV-EDV; $r = 0.96$, and bias -0.55 ± 3.2 ml for RV-ESV, and $r = 0.91$, and bias -0.36 ± 4.9 ml for RV-mass.

Discussion

This study characterizes the RV responses to chronic pressure overload. An interesting result is that the time-to-peak flow in the PA was significantly longer in animals with PAB than in healthy controls and that this parameter correlated with RV-Pmax and RV-Ped. Cine CMR findings showed that PAB-induced pressure overload increased the RV mass by 60%, increased the RV-ESV significantly, and, consequently, decreased RV-EF. Conductance

catheter-based measurements revealed that myocardial contractility of the RV rose significantly (through an increase in PRSW and ESPVR) following PAB.

Leeuwenburgh et al. [21,22] reported that chronic RV pressure overload resulted in a significant increase in RV free-wall thickness in lambs, due to a hyperplastic myocardial response. Similarly, 3 months after PAB we found that RV masses increased by 60% as compared to healthy control animals. Moreover, our conductance catheter data demonstrated a significant increase in myocardial contractility, in line with the results presented by de Vroomen et al. [23]. A few experimental studies have shown hypercontractility of the RV to be a consequence of the increased afterload, thereby maintaining ventricular-arterial coupling and RV ejection volumes [24,25]. In the study by Leeuwenburgh et al. [21], the hyperplastic myocardial response to PAB was not associated with changes in RV volumes. In our study, however, we observed that RV-ESV and, to a lesser extent, RV-EDV increased, while RV-EF decreased significantly 3 months after PAB. Boehm et al. [26] showed that the indices of RV systolic function deteriorated upon chronic pressure overload compared with sham-operated rats. Nevertheless, pressure loop-derived indices demonstrated a hypercontractile RV, even in animals with clinical signs of heart failure and ventricular-arterial decoupling. These findings are consistent with our results regarding the RV volumes and the state of hypercontractility, but our animals, in contrast, showed no clinical signs of right ventricular failure and right ventricular – arterial coupling was preserved.

Evaluation of early RV dysfunction by CMR is challenging. A promising new technique is to analyze the velocities of the atrioventricular junction, where the velocity in early diastole is a parameter of diastolic function [27]. Although diastolic dysfunction after PAB has been previously reported [28,29], our study demonstrated normal RV diastolic function based on cine CMR data (TVA-VDS, TVA-VED) and catheter data (end-diastolic elastance, maximum speed of pressure decline dP/dtmin, and end-diastolic pressure).

PC-CMR-based flow measurements comprise a wide range of parameters that characterize the pulmonary circulation [30-32]. The main result of our study was that the time-to-peak flow in the PA was significantly longer in the PAB group than in healthy controls. This also held true when comparing the differences in time-to-peak flow in the PA and aorta of both groups. Moreover, the length of the time-to-peak flow correlated with the pressure parameters RV-Pmax and RV-Ped. These findings, together with the normal RV-Pmax, RV-Pes, the decreased RV-EF, and the increased RV-ESV, may indicate incipient RV dysfunction.

Limitations

This study is subject to the following limitations. Firstly, because conductance catheter analyses were performed through different surgical access routes before and 3 months after PAB, the changes in RV-Pmax, RV-Pes, and RV-Ped after PAB could be caused by the thoracotomy method itself. This issue was addressed by Hoit et al. [33], who found that hemodynamics of the LV in rats (heart rate, Ped, dP/dtmax, dP/dtmin) during closed-chest preparation are significantly different than those in open-chest preparation. Performing sham operations in our control group would have helped to clarify the influence of access routes on the measurement results. Secondly, the number of animals in the two groups was small. Although this is a common problem in translational research programs utilizing clinically relevant large animal models, small sample sizes severely limit the statistical power of an investigation [34]. Thirdly, the low temporal resolution (40 ms) of the PC-CMR pulse sequence used for flow measurements in this study precluded estimation of mean PA pressure by calculating the absolute acceleration time [31,35]. Fourthly, the time gap between MR examination and final invasive pressure-volume examinations ranged between 7 and 10 days. It is known that there can be considerable spontaneous variations in pulmonary functional parameters even over a short period of time [36]. Simultaneous assessment of invasive cardiovascular pressures combined with MRI-derived PA blood flow and RV volumes, as proposed by Kuehne et al., should provide a solution to this problem [37]. The cross-sectional

design of this study regarding the CMR examinations represents another limitation, as the healthy controls were not the same animals in which the banding procedure was performed, excluding longitudinal comparison. However, the choice of age-matched healthy control animals excludes any growth-related influence on RV volumes.

Conclusions

Reducing the diameter of the pulmonary artery by 50% through PAB increased time-to-peak PA flow and RV mass, decreased RV-EF (assessed by CMR), and increased myocardial contractility (assessed by conductance catheter). Moreover, time-to-peak flow in the PA correlated with RV pressure parameters. Although these changes may still be indicative of the physiological adaptation process after PAB, the reduced RV-EF, the increased RV-ESV, and the prolonged time-to-peak PA flow may point to a possible incipient RV failure. Therefore, time-to-peak PA flow, RV-EF, and RV-ESV may serve as index parameters for incipient RV failure that can be obtained noninvasively by CMR and may replace, in some cases, invasive catheter measurements. Studies employing late gadolinium enhancement sequences should be conducted in the future to detect areas of fibrosis in the RV myocardium as a possible marker of PAB-induced RV remodeling.

Compliance with Ethical Standards

Funding This research received no grant from any funding agency in the public, commercial or not-for-profit sectors.

Conflict of Interest The authors declare that they have no conflict of interest.

Ethical approval This study was approved by the local Animal Care Committee. Animals received humane care in compliance with the Principles of Laboratory Animal Care

formulated by the National Society for Medical Research and the Guide for the Care and Use of Laboratory Animals.

References

1. Lacour-Gayet F, Piot D, Zoghbi J, Serraf A, Gruber P, Macé L, Touchot A, Planché C (2001). Surgical management and indication of left ventriculuar retraining in arterial switch for transposition of the great arteries with intact ventricular septum. Eur J Cardiothorac Surg;20:824-829.

2. Pinho P, Von Oppell UO, Brink J, Hewitson J (1997). Pulmonary artery banding: adequacy and long-term outcome. Eur J Cardiothorac Surg 11:105-111.

3. Metton O, Gaudin R, Ou P, Gerelli S, Mussa S, Sidi D, Vouhé P, Raisky O (2010). Early prophylactic pulmonary artery banding in isolated congenitally corrected transposition of the great arteries. Eur J Cardiothorac Surg 38:728-734.

4. Bogaard HJ, Abe K, Noordegraaf AV, Voelkel NF (2009). The right ventricle under pressure: cellular and molecular mechanisms of right-heart failure in pulmonary hypertension. Chest 135:794-804.

5. Rain S, Bos Dda S, Handoko ML, Handoko ML, Westerhof N, Stienen G, Ottenheijm C, Goebel M, Dorfmüller P, Guignabert C, Humbert M, Bogaard HJ, Remedios CD, Saripalli C, Hidalgo CG, Granzier HL, Vonk-Noordegraaf A, van der Velden J, de Man FS (2014). Protein changes contributing to right ventricular cardiomyocyte

diastolic dysfunction in pulmonary arterial hypertension. J Am Heart doi: 10.1161/JAHA.113.000716.

6. Rain S, Andersen S, Najafi A, Gammelgaard Schultz J, da Silva Goncalves Bos D, Handoko ML, Bogaard HJ, Vonk-Noordegraaf A, Andersen A, van der Velden J, Ottenheijm CA, de Man FS (2016). Right ventricular myocardial stiffness in experimental pulmonary arterial hypertension: relative contribution of fibrosis and myofibril stiffness. Circulation Heart failure doi: 10.1161/CIRCHEARTFAILURE. 115.002636.

7. Noly PE, Haddad F, Arthur-Ataam J, Langer N, Dorfmüller P, Loisel F, Guihaire J, Decante B, Lamrani L, Fadel E, Mercier O (2017). The importance of capillary density-stroke work mismatch for right ventricular adaptation to chronic pressure overload. J Thorac Cardiovasc Surg 154:2070-2079.

8. Maughan WL, Sunagawa K, Sagawa K (1987). Ventricular systolic interdependence: volume elastance model in isolated canine hearts. Am J Physiol 253:H1381–H1390.

9. Borgdorff MAJ, Dickinson MG, Berger RMP, Bartelds B (2015). Right ventricular failure due to chronic pressure load: what have we learned in animal models since the NIH working group statement? Heart Fail Rev 20:475-491.

10. Burkhoff D, Mirsky I, Suga H (2005). Assessment of systolic and diastolic ventricular properties via pressure-volume analysis: a guide for clinical, translational, and basic researchers. Am J Physiol Heart Circ Physiol 289:H501-H512.

11. Faber MJ, Dalinghaus M, Lankhuizen IM, Steendijk P, Hop WC, Schoemaker RG, Duncker DJ, Lamers JM, Helbing WA (2006). Right and left ventricular function after chronic pulmonary artery banding in rats assessed with biventricular pressure-volume loops. Am J Physiol Heart Circ Physiol 291:H1580–H1586.

12. Vogel M (1999). The optimal method with which to assess right ventricular function. Cardiol Young 9:547–548.

13. Schmitt B, Steendijk P, Lunze K, Ovroutski S, Falkenberg J, Rahmanzadeh P, Maarouf N, Ewert P, Berger F, Kuehne T (2009). Integrated assessment of diastolic and systolic ventricular function using diagnostic cardiac magnetic resonance catheterization: validation in pigs and application in a clinical pilot study. JACC Cardiovasc Imaging 2:1271-1281.

14. Yu CM, Sanderson JE, Marvick TH, Oh JK (2007). Tissue Doppler imaging a new prognosticator for cardiovascular disease. JACC 49:1903-1934.

15. Hollingsworth KG, Hodgson T, MacGowan GA, Blamire AM, Newton JL (2011). Impaired cardiac function in chronic fatigue syndrome measured using magnetic resonance cardiac tagging. J Intern Med 271:264-278.

16. Jing L, Pulenthiran A, Nevius CD, Mejia-Spiegeler A, Suever JD, Wehner GJ, Kirchner HL, Haggerty CM, Fornwalt BK (2017). Impaired right ventricular contractile function in childhood obesity and its association with right and left ventricular changes: a cine DENSE cardiac magnetic resonance study. J Cardiovasc Magn Reson doi: 10.1186/s12968-017-0363-5.

17. Le Bret E, Bonhoeffer P, Folliguet TA, Sidi D, Laborde F, de Leval MR, Vouhé P (2001). A new percutaneously adjustable, thoracoscopically implantable, pulmonary artery banding: an experimental study. Ann Thorac Surg 72:1358-61.

18. Alam M, Wardell J, Andersson E, Samad BA, Nordlander R (2000). Right ventricular function in patients with first inferior myocardial infarction: assessment by tricuspid annular motion and tricuspid annular velocity. Am Heart J 139:710-715.

19. Saba SG, Chung S, Bhagavatula S, Donnino R, Srichai MB, Saric M, Katz SD, Axel L (2014). Novel and practical cardiovascular magnetic resonance method to quantify mitral annular excursion and recoil applied to hypertrophic cardiomyopathy. J Cardiovasc Magn Reson 16:35-43.

20. Wu V, Chyou JY, Chung S, Bhagavatula S, Axel L (2014). Evaluation of diastolic function by three-dimensional volume tracking of the mitral annulus with cardiovascular magnetic resonance: comparison with tissue Doppler imaging. *J Cardiovasc Magn Reson* **16**:71-84.

21. Leeuwenburgh BP, Steendijk P, Helbing WA, Baan J (2002). Indexes of diastolic RV function: load dependence and changes after chronic RV pressure overload in lambs. Am J Physiol Heart Circ Physiol 282:H1350–H1358.

22. Leeuwenburgh BPJ, Helbing WA, Steendijk P, Schoof PH, Baan J (2001). Biventricular systolic function in young lamb subject to chronic systemic right ventricular pressure overload. Am J Physiol Heart Circ Physiol 281:H2697–H2704.

23. de Vroomen M, Cardozo RH, Steendijk P, van Bel F, Baan J (2000). Improved contractile performance of right ventricle in response to increased RV afterload in newborn lamb. Am J Physiol Heart Circ Physiol 278:H100–H105.

24. Fesler P, Pagnamenta A, Rondelet B, Kerbaul F, Naeije R (2000). Effects of sildenafil on hypoxic pulmonary vascular function in dogs. J Appl Physiol 101:1085-1090.

25. Rex S. Missant C, Segers P, Roussaint R, Wourters PP (2008). Epoprostenol treatment of acute pulmonary hypertension is associated with a paradoxical decrease in right ventricular contractility. Intensive Care Med 34:179-189.

26. Boehm M, Lawrie A, Wilhelm J, Ghofrani HA, Grimminger F, Weissmann N, Seeger W, Schermuly RT, Kojonazarov B (2017). Maintained right ventricular pressure overload induces ventricular-arterial decoupling in mice. Exp Physiol 102:180-189.

27. Ito S, McElhinney, Adams R, Bhatla P, Chung S, Axel L (2015). Preliminary assessment of tricuspid valve annular velocity parameters by cardiac magnetic resonance imaging in adults with a volume-overloaded right ventricle: comparison of unrepaired atrial septal defect and repaired tetralogy of Fallot. Pediatr Cardiol 36:1294-1300.

28. Borgdorff MA, Bartelds B, Dickinson MG, Boersma B, Weij M, Zandvoort A, Sillje HH, Steendijk P, de Vroomen M, Berger RM (2012). Sildenafil enhances systolic adaptation, but does not prevent diastolic dysfunction, in the pressure-loaded right ventricle. Eur J Heart Fail 14:1067–1074.

29. Gaynor SL, Maniar HS, Bloch JB, Steendijk P, Moon MR (2005). Right atrial and ventricular adaptation to chronic right ventricular pressure overload. Circulation 112:I212–I218.

30. Sanz J, Kuschnir P, Rius T, Salguero R, Sulica R, Einstein AJ, Dellegrottaglie S, Fuster V, Rajagopalan S, Poon M (2007). Pulmonary arterial hypertension: noninvasive detection with phase-contrast MR Imaging. Radiology 243:70-79.

31. Abolmaali N, Seitz U, Esmaeili A, Kock M, Radeloff D, Ackermann H, Vogl TJ (2007). Evaluation of a resistance-based model for the quantification of pulmonary arterial hypertension using MR flow measurements. J Magn Reson Imaging 26:646-653.

32. García-Alvarez A, Fernández-Friera L, Mirelis JG, Sawit S, Nair A, Kallman J, Fuster V, Sanz J (2011). Non-invasive estimation of pulmonary vascular resistance with cardiac magnetic resonance. Eur Heart J 32:2438-2445.

33. Hoit BD, Ball N, Walsh RA (1997). Invasive hemodynamics and force-frequency relationships in open- versus closed-chest mice. Am J Physiol 273:H2528-H2533.

34. Boltze J, Förschler A, Nitzsche B, Waldmin D, Hoffmann A, Boltze CM, Dreyer AY, Goldammer A, Reischauer A, Härtig W, Geiger KD, Barthel H, Emmrich F, Gille U (2008). Permanent middle cerebral artery occlusion in sheep: a novel large animal model of focal cerebral ischemia. J Cereb Blood Flow Metab 28:1951-1964.

35. Kreitner KF, Wirth GM, Krummenauer F, Weber S, Pitton MB, Schneider J, Mayer E, Dueber C (2013). Noninvasive assessment of hemodynamics in patients with thromboembolic pulmonary hypertension by high temporal resolution phase-contrast MRI: correlation with simultaneous invasive pressure recordings. Circ Cardiovasc Imaging 6:722-729.

36. Schrijen F, Jezkov J (1988). Natural variability of pulmonary hemodynamics. Eur Heart J 9:19-22.

37. Kuehne T, Yilmaz S, Steendijk P, Moore P, Groenink M, Saaed M, Weber O, Higgins CB, Ewert P, Fleck E, Nagel E, Schulze-Neick I, Lange P (2004). Magnetic Resonance imaging analysis of right ventricular pressure-volume loops in vivo validation and clinical application in patients with pulmonary hypertension. Circulation 110:2010-2016.

Table and Figure Legends

Figure 1 Flow pattern in the pulmonary artery throughout the cardiac cycle in pulmonary artery banding group (red line) and controls (black dashed line). Rightward shift of the time-to-peak flow in the PAB group (blue arrow)

Figure 2 Correlation between time-to-peak flow in the pulmonary artery and end-diastolic pressure (RV-Ped) in panel A and maximal right ventricular pressure (RV-Pmax) in panel B in animals after pulmonary artery banding. TTP = Time-to-peak

Table 1 Conductance catheter-based measurements before and 3 months after pulmonary artery banding

Table 2 Right and left ventricular volume measurements derived from cine cardiac magnetic resonance

Figure 1

Click here to access/download;Figure;Figure 1.tif

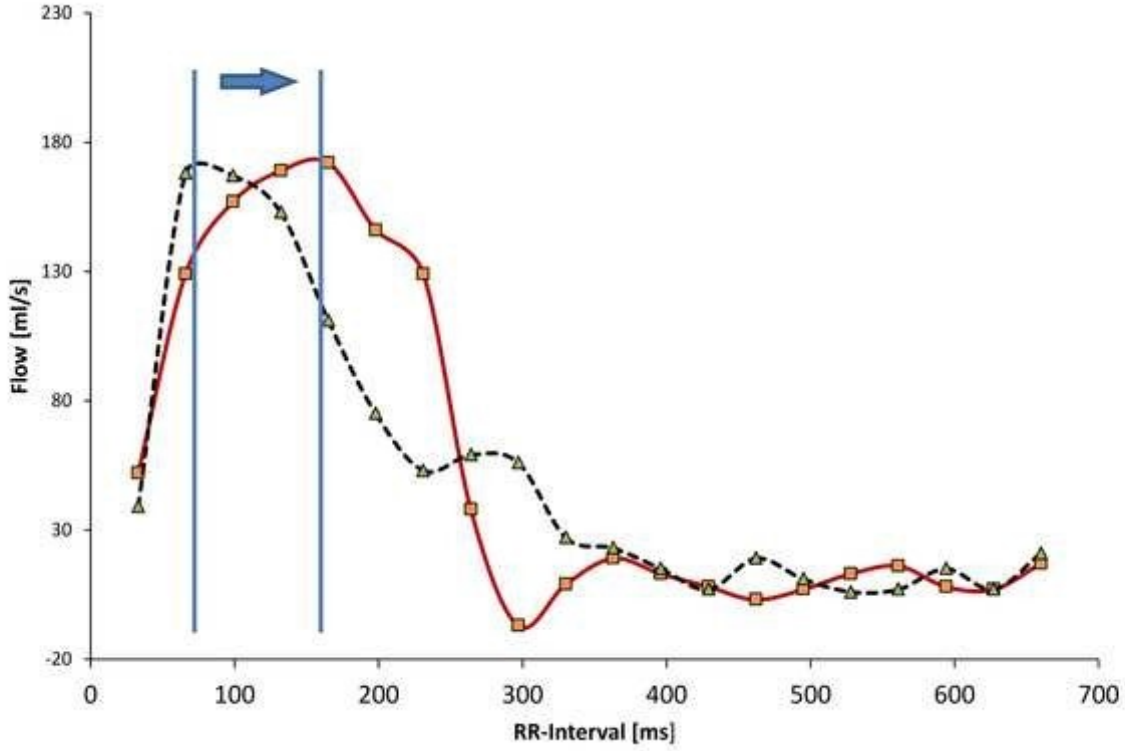

Figure 2

Click here to access/download;Figure;Figure 2.tif

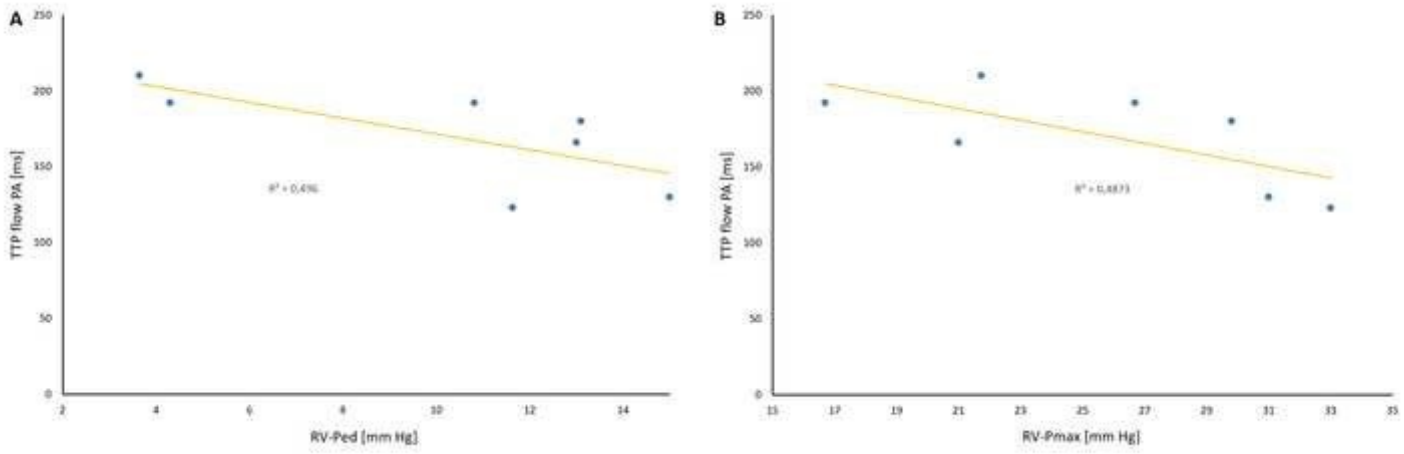

Table 1: Conductance catheter-based measurements before and 3 months after pulmonary artery banding

	Before PAB (n = 7)	After PAB (n = 7)	p Value
Heart rate, min^{-1}	79.4 ± 11.5	77.41 ± 11.79	0.56
RV-CO, ml·min	3448.16 ± 904.57	2220.63 ± 552.4	**< 0.003**
RV-Pmax, mmHg	25.49 ± 3.08	20.91 ± 3.86	< 0.06
RV-Ped, mmHg	9.37 ± 3.39	4.61 ± 3.41	**< 0.06**
RV-Pes, mmHg	18.1 ± 3.45	16.46 ± 4.19	0.22
RV-dP/dtmax, mmHg/s	334.74 ± 77.94	318.18 ± 111.86	0.63
RV-dP/dtmin, mmHg/s	-324.73 ± 59.91	-296.10 ± 12.85	0.37
RV-ESPVR	0.52 ± 0.18	1.34 ± 0.58	**< 0.005**
RV-EDPVR	0.20 ± 0.07	0.11 ± 0.09	**< 0.007**
RV-PRSW, mmHg·ml	12.85 ± 4.71	16.83 ± 5.93	**< 0.04**
Ees, mmHg/ml	0.48 ± 0.18	1.63 ± 1.28	**< 0.03**
Ea, mmHg/ml	0.45 ± 0.14	0.69 ± 0.38	0.07
Ees/Ea	1.07 ± 0.37	2.36 ± 1.41	**< 0.03**

RV-CO = right ventricular cardiac output; RV-Pmax = right ventricular maximal pressure; RV-Ped = right ventricular end-diastolic pressure; RV-Pes = right ventricular end-systolic pressure; RV-dP/dtmax = maximal right ventricular pressure change; RV-dP/dtmin = minimal right ventricular pressure change; RV-ESPVR = right ventricular end-systolic pressure volume relationship; RV-EDPVR = right ventricular end-diastolic pressure volume relationship; RV-PRSW = right ventricular pressure related stroke work. Ees = end-systolic elastance; Ea = arterial elastance

Table 2. Right and left ventricular volume measurements derived from cine cardiac magnetic resonance. Values normalized to body weight in parenthesis.

	PAB Group (n = 7)	Healthy controls (n = 4)	p Value
RV Volumes			
RV-ESV, ml	37.1 ± 7.5	19.3 ± 3.8	**< 0.05**
	(0.95 ± 0.13)	(0.45 ± 0.08)	**(< 0.01)**
RV-EDV, ml	82.6 ± 16.8	66.0 ± 24.0	0.37
	(2.12 ± 0.37)	(1.60 ± 0.38)	(0.06)
RV-SV, ml	46.8 ± 12.9	57.5 ± 2.1	0.30
	(1.17 ± 0.29)	(1.22 ± 0.30)	(0.72)
RV-EF, %	54.2 ± 5.3	71.1 ± 4.8	**< 0.01**
RV-mass, g	39.2 ± 5.8	23.5 ± 4.3	**< 0.01**
	(1.12 ± 0.13)	(0.55 ± 0.11)	**(< 0.001)**
LV Volumes			
LV-ESV, ml	55.9 ± 12.2	35.9 ± 6.4	0.07
	(1.40 ± 0.30)	(0.93 ± 0.30)	(0.06)
LV-EDV, ml	102.9 ± 11.7	81.9 ± 20.5	0.13
	(2.58 ± 0.28)	(1.93 ± 0.45)	(0.06)
LV-SV, ml	47.1 ± 1.9	46.6 ± 15.5	0.95
	(1.18 ± 0.29)	(1.09 ± 0.35)	(0.71)
LV-EF, %	40.9 ± 10.0	46.1 ± 6.5	0.06
LV-mass, g	85.2 ± 9.8	73.5 ± 14.5	0.21
	(2.14 ± 0.28)	(1.73 ± 0.34)	(0.10)